GEOCHRONOMETRIA 52 (2025) 205688
DOI 10.20858/geochr/205688

Available online at https://www.geochronometria.com/

A FIRST CHRONOLOGICAL FRAMEWORK FOR FLUVIAL TERRACE DEPOSITS OF THE KAMPAR KANAN RIVER, INDONESIA

YUNIARTI YUSKAR[1, 4], MELANIE KRANZ-BARTZ[3], CHRISTOPH SCHMIDT[1], TIGGI CHOANJI[2, 4], STUART N. LANE[1] and GEORGINA E. KING[1]

[1]Institute of Earth Surface Dynamics, University of Lausanne, 1015 Lausanne, Switzerland
[2]Institute of Earth Science, University of Lausanne, 1015 Lausanne, Switzerland
[3]Institute of Geosciences, Ruhr University Bochum, 44801 Bochum, Germany
[4]Department of Geological Engineering, Universitas Islam Riau, 28284 Pekanbaru, Indonesia

SUPPLEMENTARY MATERIALS

Raman spectroscopy

Raman spectroscopy uses a Raman spectrometer with high spectral resolution coupled to a Leica confocal microscope. The equipment includes four interchangeable diffraction gratings (1200 to 3000 l/mm), two lasers (Nd:YAG 532 nm and 785 nm lasers) and a CCD detector (1024 × 256 pixels). It allows point analyses or 2D and 3D maps of micro- and macro-samples.

Table S1. *Analysis of mineral identification by Raman spectroscopy (KFS = K-feldspar).*

Sample code	Total grains	Quartz	Feldspar		Un-identified minerals	% of KFS
			Alkali feldspar	Plagioclase		
L1	200	195	1	-	4	1
L3	75	65	4	4	2	5
L6	75	51	4	3	16	5

XRF results

Table S2. *Analysis of mineral identification by XRF. Assuming that Na and K-feldspar emit luminescence in the blue part of the emission spectrum, and that quartz does not respond to infrared stimulation, we have scaled the K content of the samples relative to the proportions of K- and Na-feldspar, on the basis of an assumed K content of 12.5% in K-feldspar minerals (e.g. Huntley and Baril, 1997). As our samples contain very little feldspar, and consequently our XRF measurements may be biased by the presence of only a few feldspar grains, we have calculated an average K content across all of the samples investigated.*

Sample Code	Measurement number	F+Q on mass				Ratio of K-F to K-F + Na-F	K content	Average K content	Uncertainty
		Na-F	K-F	Ca-F	Q				
L1	1	0.000	0.010	0.000	1.018	1.000	12.500	12.50	0.00
	3	0.000	0.013	0.002	0.987	1.000	12.500		
L2	2	0.007	0.016	0.004	0.974	0.696	8.696	8.15	0.77
	3	0.009	0.014	0.002	0.976	0.609	7.609		
L3	2	0.012	0.002	0.002	0.984	0.143	1.786	7.14	7.58
	3	0.000	0.002	0.001	1.005	1.000	12.500		
L4	1	0.006	0.001	0.000	0.993	0.143	1.786	8.93	7.58
	2	0.000	0.007	0.003	0.992	1.000	12.500		
	3	0.000	0.012	0.000	0.996	1.000	12.500		
L5	1	0.005	0.006	0.000	0.989	0.545	6.818	6.03	2.83
	2	0.048	0.014	0.001	0.938	0.226	2.823		
	3	0.027	0.056	0.001	0.915	0.675	8.434		
L6	3	0.025	0.027	0.001	0.947	0.519	6.490	6.49	0.000
L7	2	0.015	0.019	0.002	0.965	0.559	6.985	9.74	0.35
	3	0.000	0.024	0.002	0.996	1.000	12.500		
							Site averaged K-content	8.43	2.23

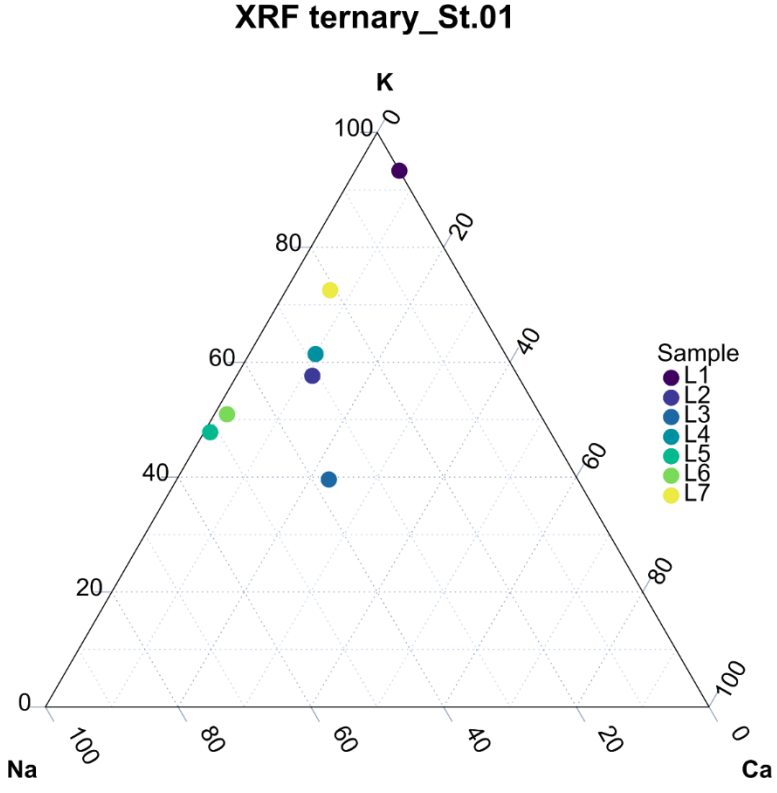

Fig. S1. *Phase diagram of feldspar samples (L1 to L7) investigated. Composition determined from X-ray fluorescence spectroscopy (XRF).*

Table S3. *General SAR protocol, double SAR protocol and pIR-IRSL protocol.*

General SAR protocol (after Murray and Wintle, 2000)			Double SAR protocol (Roberts and Wintle, 2001; Banerjee *et al*., 2001).		SAR Protocol of $pIR_{50}IRSL_{225}$ K-FS (Thomsen *et al.*, 2008, Bartz *et al.*, 2020)	
Step	**Treatment**	**Observed**	**Treatment**	**Observed**	**Treatment**	**Observed**[d]
1	Give dose, D_i	—	1. Natural dose and give dose, D_i	—	1. Give dose, D_i	—
2	Preheat (160–300°C) for 10 s	—	2. Preheat (240°C for 10 s)	—	2. Preheat (250°C) for 60 s	—
3	Stimulation for 100 s at 125 °C	L_i	3. IR stimulation for 500 s at 50°C	L_i	3. IR stimulation for 180 s at 50°C	L_i at 50°C
4	Give test dose, D_t	—	4. Green or blue stimulation for 40 s at 125°C	L_i	4. pIR-IRSL stimulation for 180 s at 225°C	L_i at 225°C
5	Heat[b] to 160°C	—	5. Give test dose, D_t (13.2 Gy)	—	5. Give test dose, D_t	—
6	Stimulate for 100 s at 125°C	T_i	6. Heat to 200°C	—	6. Heat to 250°C for 60 s	—
7	Return to step 1	—	7. IR stimulation for 500 s at 50°C	T_i	7. IR stimulation for 180 s at 50°C	T_i at 50°C
			8. Green or blue stimulation for 40 s at 125°C	T_i	8. pIR-IR stimulation for 180 s at 225°C	T_i at 225°C
			9. Return to step 1	—	9. IR stimulation for 100 s at 290°C	—
					10. Return to step 1	

Deconvolution of quartz CW- and LM-OSL curves

Methodology

Aliquots of samples L3 and L4 were analysed to check for a dominant fast component in the OSL signals. For this, we used CW-OSL curve deconvolution for OSL signals measured with blue (80 mW cm^{-2}, 470 nm; Bøtter-Jensen *et al.*, 2010) light emitting diodes at 90% LED power and with green (50 mW cm^{-2}, 525 nm, Lapp *et al.*, 2015) light emitting diodes at 60% LED power. For the green diodes, we also conducted a LM-OSL experiment, varying the LED power from 0 to 60%. CW- and LM-OSL curves were decomposed using the `fit_CWcurve()` and `fit_LMcurve()` functions in the R package 'Luminescence' (0.9.22; Kreutzer *et al.*, 2023a, 2023b).

Results

CW-OSL signal decomposition of the natural and regenerative OSL signals yielded either weak or no fast component, with mainly medium or slow components. A representative aliquot of sample L3 yielded two components with photoionisation cross-sections on the order of 10^{-18} and 10^{-20} cm^2 (**Fig. S2** left), with a moderate goodness-of-fit value of 0.936 (**Fig. S2**). The regenerative signal of sample L3 showed a better fit with a pseudo r^2 value of 0.999, but with similar trap parameters and photoionisation cross-sections, indicating a medium and slow component rather than a dominant fast component. Using green LED stimulation, CW-OSL signal decomposition revealed a weak fast component (**Fig. S2** right) contributing only ~25% to the total OSL signal (component 1), while the medium (component 2) and two slow components (components 3 and 4) dominate the OSL signal. Sample L4 showed similar results. LM-OSL curve deconvolution showed no fast component, in agreement with CW-OSL curve fitting (**Fig. S3**).

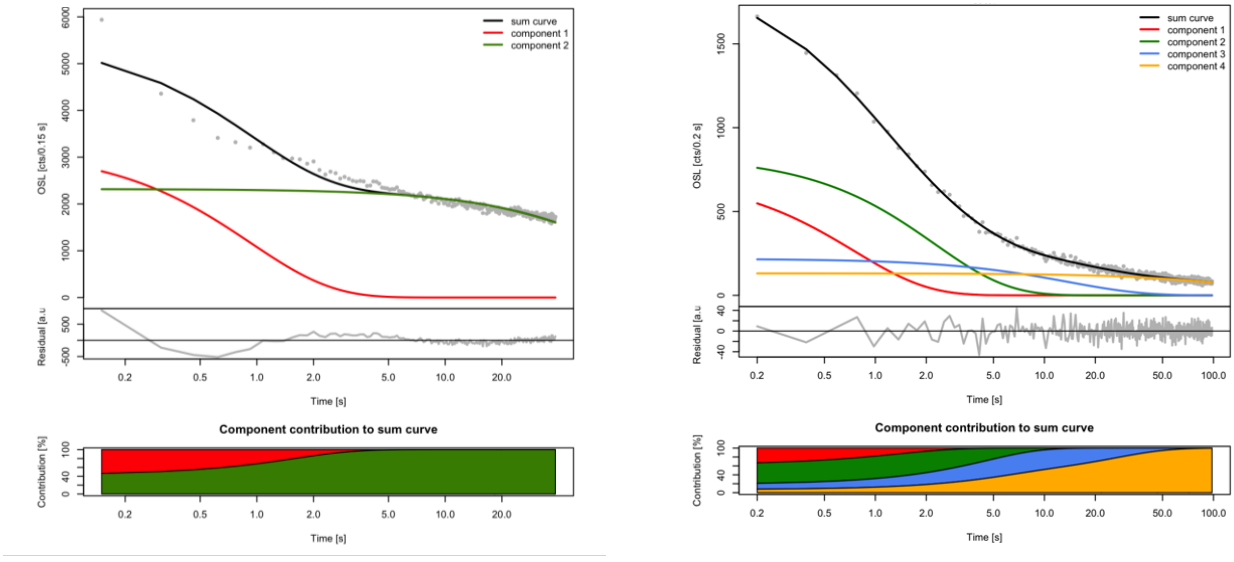

Fig. S2. *Exemplary CW-OSL signal decomposition of sample L3 using blue (left) and green (right) stimulation. Based on the trap parameters and photoionization-cross sections: left - component 1 = medium component, component 2 = slow component. Right - component 1 = fast component, component 2 = medium component, components 3 and 4 = slow components.*

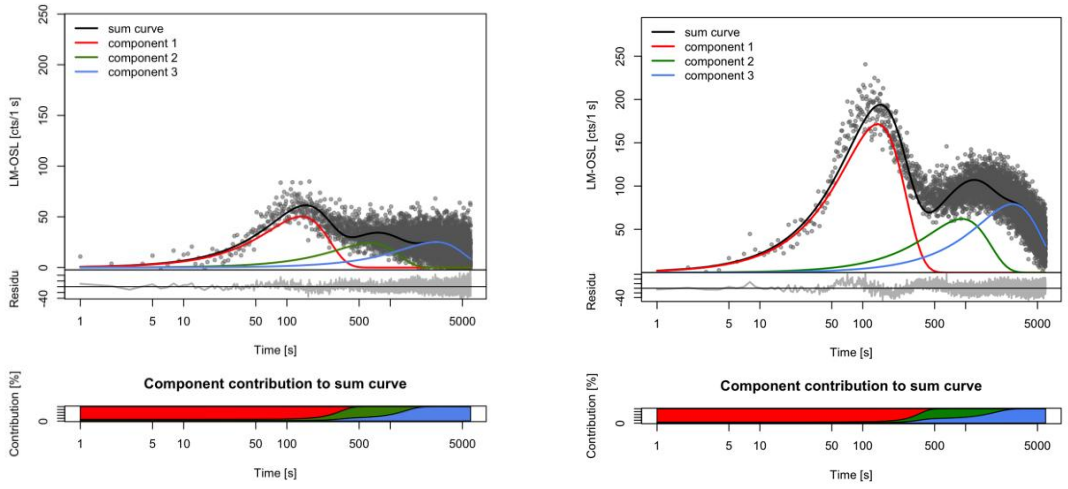

Fig. S3. *LM-OSL curve decomposition of samples L3 (left) and L4 (right). Based on the trap parameters and photoionization-cross sections: component 1 = medium component, component 2 and 3 = slow components.*

Supplementary result of D_e comparison with different sigma-b values.

Table S4. *D_e comparison with different sigma-b values.*

IR50									
Sample Code	** σ_b	D_e (Gy)		** σ_b	D_e (Gy)		** σ_b	D_e (Gy)	
		MAM	ADM		MAM	ADM		MAM	ADM
L7	0.21	4.42 ± 0.68	14.28 ± 1.72	0.30	4.84 ± 0.86	13.96 ± 1.81	0.40	5.45 ± 1.15	13.48 ± 1.54
L6	0.21	6.64 ± 0.95	9.06 ± 0.89	0.30	6.64 ± 0.95	8.85 ± 0.83	0.40	7.78 ± 0.57	8.55 ± 0.82
L5	0.21	10.45 ± 1.60	53.24 ± 6.93	0.30	12.80 ± 2.24	52.04 ± 6.30	0.40	15.03 ± 3.16	50.24 ± 6.58
L4	0.21	10.00 ± 2.47	189.81 ± 18.72	0.30	13.99 ± 3.83	185.50 ± 18.52	0.40	21.7 ± 6.74	179.12 ± 17.50
L3	0.21	27.04 ± 5.39	197.30 ± 15.94	0.30	40.40 ± 9.86	192.83 ± 17.35	0.40	65.43 ± 17.31	186.19 ± 15.21
L2	0.21	278.93 ± 38.77	369.80 ± 29.00	0.30	345.03 ± 48.49	361.41 ± 28.23	0.40	362.51 ± 51.23	362.51 ± 27.02
L1	0.21	147.69 ± 16.49	245.95 ± 15.74	0.30	173.24 ± 25.67	240.37 ± 15.72	0.40	233.05 ± 28.70	233.05 ± 14.74

$pIR_{50}IRSL_{225}$									
Sample Code	** σ_b	D_e (Gy)		** σ_b	D_e (Gy)		** σ_b	D_e (Gy)	
		MAM	ADM		MAM	ADM		MAM	ADM
L7	0.21	14.96 ± 2.08	34.00 ± 4.70	0.30	18.01 ± 2.58	33.22 ± 4.79	0.40	19.96 ± 2.90	32.08 ± 4.73
L6	0.21	27.01 ± 1.45	27.82 ± 0.90	0.30	27.01 ± 1.34	27.82 ± 0.87	0.40	27.81 ± 2.23	27.82 ± 0.84
L5	0.21	30.35 ± 3.59	57.40 ± 6.17	0.30	33.75 ± 4.71	56.10 ± 6.45	0.40	36.55 ± 5.91	54.17 ± 6.12
L4	0.21	33.74 ± 5.80	223.23 ± 23.59	0.30	38.21 ± 8.60	218.17 ± 23.88	0.40	49.75 ± 14.19	210.66 ± 21.83
L3	0.21	74.39 ± 15.36	203.19 ± 27.29	0.30	86.70 ± 20.70	198.58 ± 27.15	0.40	101.07 ± 28.48	191.75 ± 28.00
L2	0.21	242.28 ± 55.87	489.15 ± 60.71	0.30	307.74 ± 87.82	478.05 ± 65.72	0.40	391.94 ± 100.12	461.61 ± 62.46
L1	0.21	180.49 ± 37.31	304.31 ± 38.26	0.30	208.35 ± 51.98	297.41 ± 36.87	0.40	278.08 ± 63.06	287.18 ± 38.42

Table S5. *Environmental dose rate comparison using different internal K-content of K-feldspar.*

Sample Code	Environmental dose rate (Gy ka^{-1})			
	K content = 12.5%	K content = 8%	K content = 5%	K content = 2%
L7	1.93 ± 0.27	1.71 ± 0.19	1.57 ± 014	1.42 ± 0.10
L6	1.95 ± 0.28	1.74 ± 0.19	1.59 ± 0.14	1.45 ± 0.11
L5	2.12 ± 0.09	1.88 ± 0.08	1.72 ± 0.07	1.56 ± 0.07
L4	1.66 ± 0.07	1.42 ± 0.06	1.26 ± 0.05	1.10 ± 0.05
L3	1.65 ± 0.07	1.41 ± 0.06	1.25 ± 0.06	1.08 ± 0.05
L2	2.41 ± 0.09	2.17 ± 0.08	2.01 ± 0.08	1.85 ± 0.08
L1	1.46 ± 0.07	1.22 ± 0.05	1.06 ± 0.05	0.90 ± 0.04

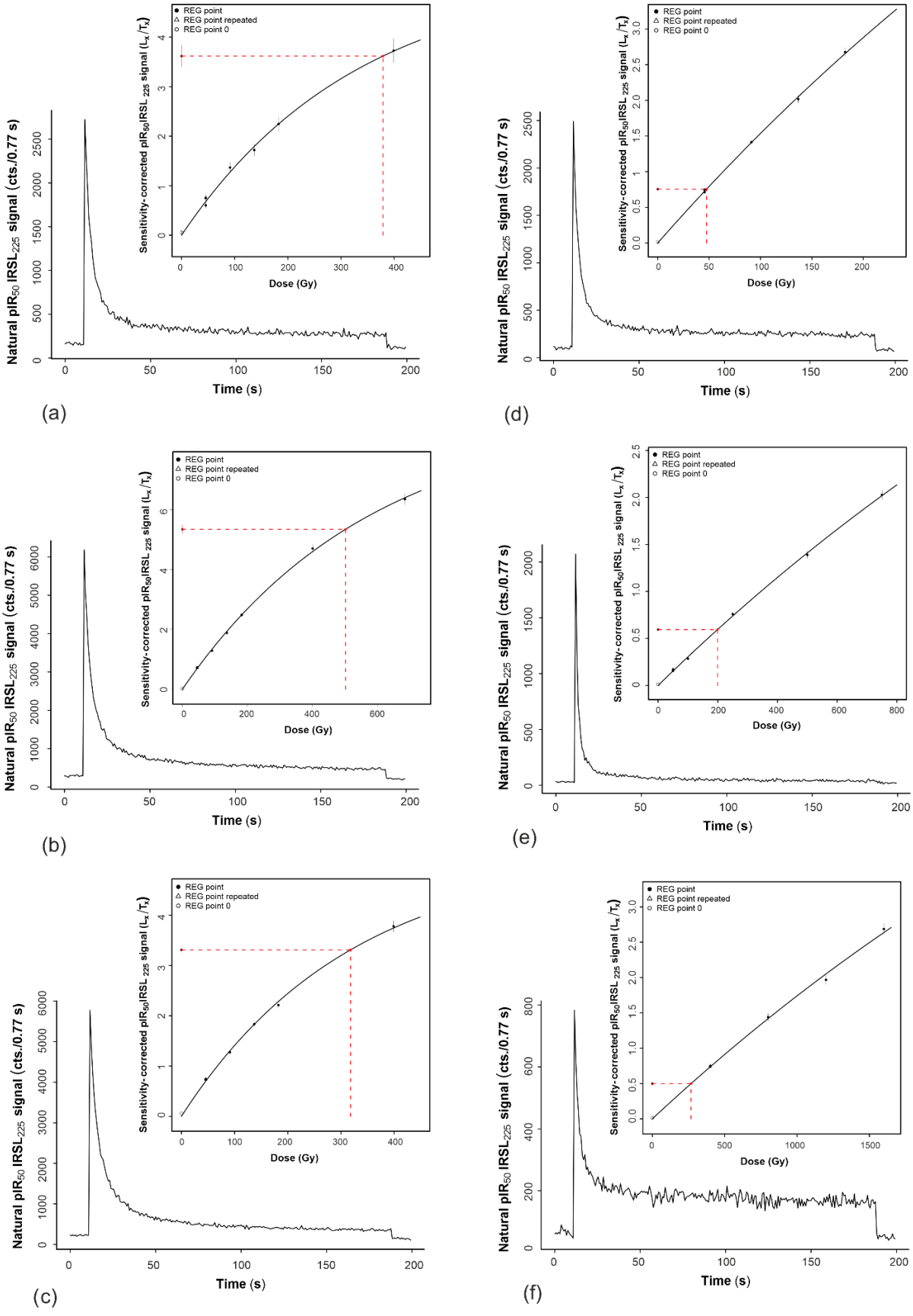

Fig. S4. *K-feldspar decay curves and dose response curves (a – b for Sample L1 and L2; c – f for sample L4 – L7).*

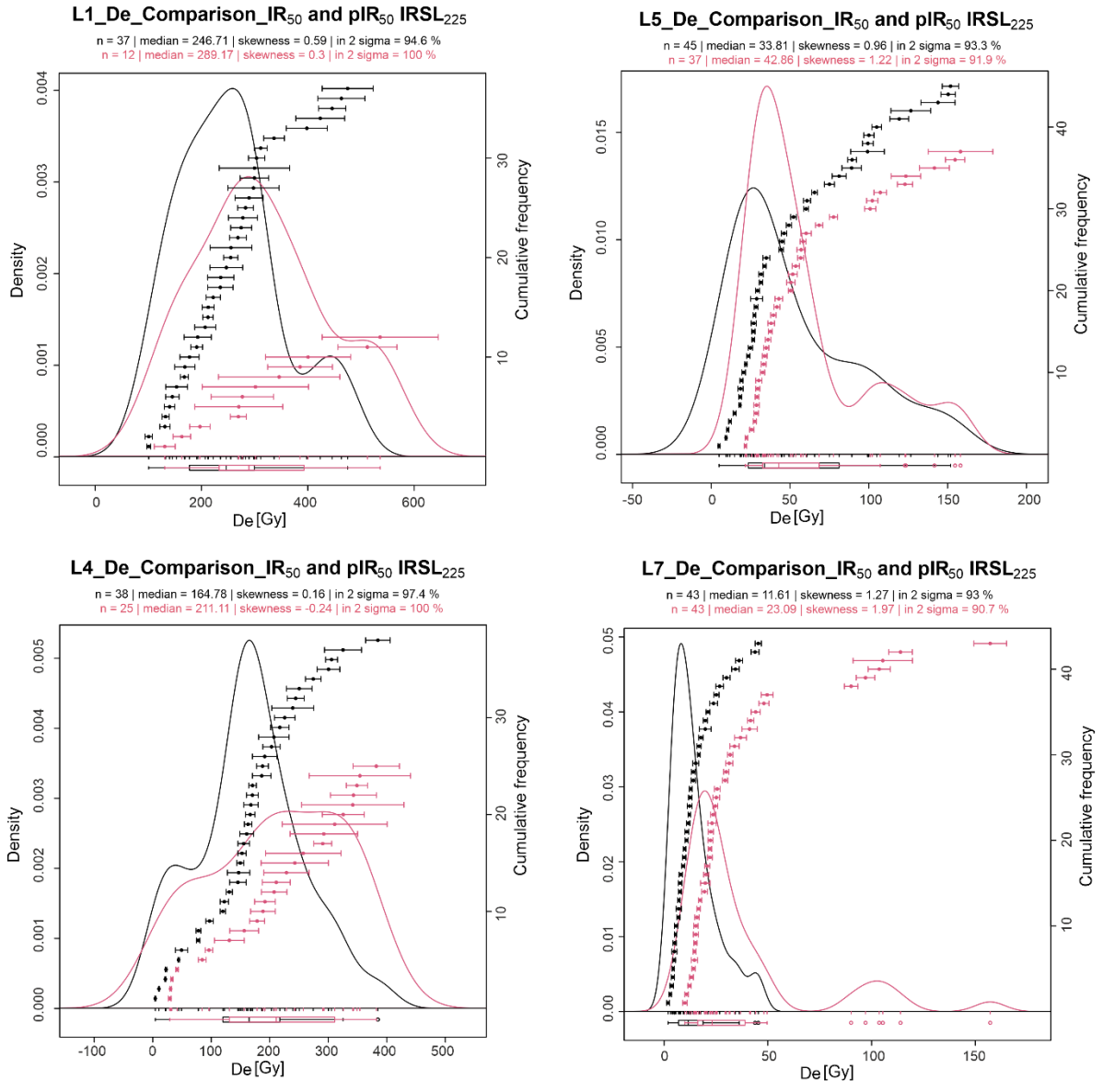

Fig. S5. *D_e comparison for IR_{50} and $pIR_{50}IRSL_{225}$ signals of samples L1, L4, L5, L6, L7.*

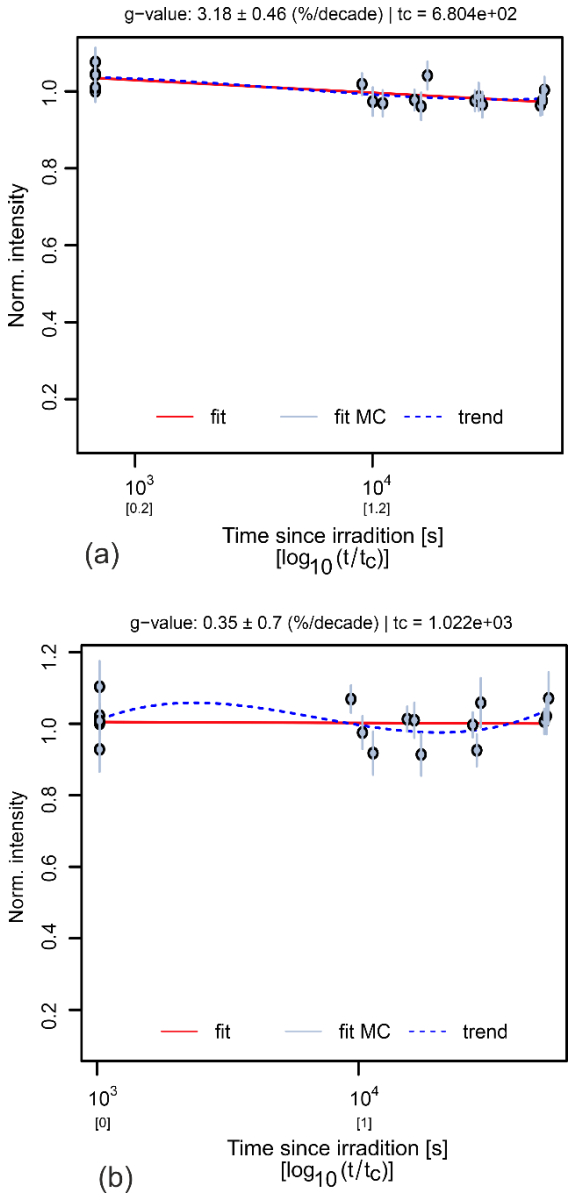

Fig. S6. *Fading measurement analysis from three aliquots of sample L1 (a: IR_{50} signal; b: $pIR_{50}IRSL_{225}$).*

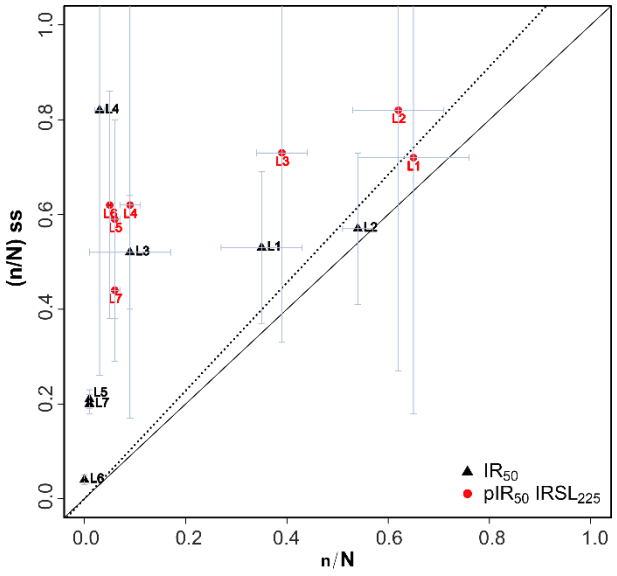

Fig. S7. *Comparison of (n/N) and $(n/N)_{ss}$ for the IR_{50} and pIR_{50} $IRSL_{225}$ signals to evaluate sample saturation. Values that sit on the solid 1:1 line, and those >86% of saturation (dotted line) are in athermal steady-state and are saturated (data summarised in Table 2; after Kars et al., 2008).*

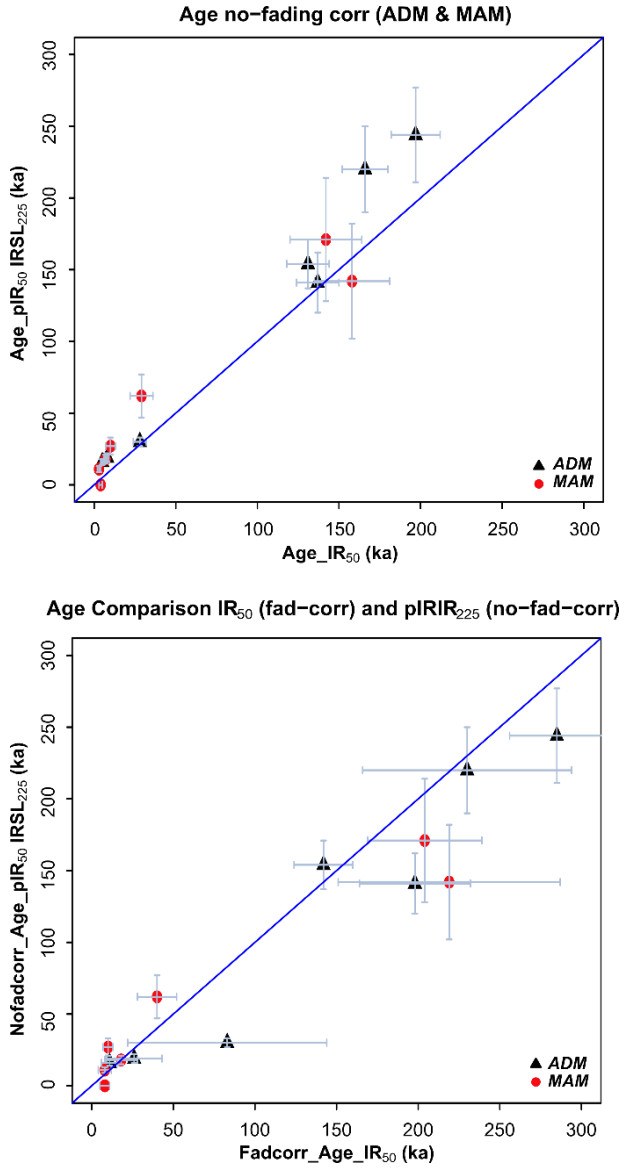

Fig. S8. *Comparison of IR_{50} and $pIR_{50}IRSL_{225}$ ages calculated with the ADM and the MAM. (a) Ages without fading correction; (b) IR_{50} ages (fading-corrected) and $pIR_{50}IRSL_{225}$ ages (not fading-corrected).*

References

Banerjee D, Murray AS, Bøtter-Jensen L and Lang A, 2001. Equivalent dose estimation using a single aliquot of polymineral fine grains. *Radiation Measurements* 33(1): 73–94, DOI 10.1016/S1350-4487(00)00101-3.

Bartz M, Duval M, Brill D, Zander A, King GE, Rhein A, Walk J, Stauch G, Lehmkuhl F and Brückner H, 2020. Testing the potential of K-feldspar pIR-IRSL and quartz ESR for dating coastal alluvial fan complexes in arid environments. *Quaternary International* 556: 124–143, DOI 10.1016/j.quaint.2020.03.037.

Bøtter-Jensen L, Thomsen KJ and Jain M, 2010. Review of optically stimulated luminescence (OSL) instrumental developments for retrospective dosimetry. *Radiation Measurements* 45(3–6): 253–257, DOI 10.1016/j.radmeas.2009.11.030.

Huntley DJ and Baril MR, 1997. The K content of the K-feldspars being measured in optical dating or in thermoluminescence dating. *Ancient TL* 15(1): 11–13, DOI 10.26034/la.atl.1997.271.

Kars RH, Wallinga J and Cohen KM, 2008. A new approach towards anomalous fading correction for feldspar IRSL dating — tests on samples in field saturation. *Radiation Measurements* 43(2–6): 786–790, DOI 10.1016/j.radmeas.2008.01.021.

Kreutzer S, 2023a. fit_CWCurve(): Nonlinear Least Squares Fit for CW-OSL curves -beta version-. Function version 0.5.2. In: Kreutzer, S, Burow, C, Dietze, M, Fuchs, M.C, Schmidt, C, Fischer, M, Friedrich, J, Mercier, N, Philippe, A, Riedesel, S, Autzen, M, Mittelstrass, D, Gray, H.J, Galharret, J, 2023. Luminescence: Comprehensive Luminescence Dating Data Analysis. R package version 0.9.22. https://CRAN.R-project.org/package=Luminescence.

Kreutzer S, 2023b. fit_LMCurve(): Nonlinear Least Squares Fit for LM-OSL curves. Function version 0.3.4. In: Kreutzer, S, Burow, C, Dietze, M, Fuchs, M.C, Schmidt, C, Fischer, M, Friedrich, J, Mercier, N, Philippe, A, Riedesel, S, Autzen, M, Mittelstrass, D, Gray, H.J, Galharret, J, 2023. Luminescence: Comprehensive Luminescence Dating Data Analysis. R package version 0.9.22. https://CRAN.R-project.org/package=Luminescence.

Lapp T, Kook M, Murray AS, Thomsen KJ, Buylaert J-P and Jain M, 2015. A new luminescence detection and stimulation head for the Risø TL/OSL reader. *Radiation Measurements* 81: 178–184, DOI 10.1016/j.radmeas.2015.02.001.

Murray AS and Wintle AG, 2000. Luminescence dating of quartz using an improved single-aliquot regenerative-dose protocol. *Radiation Measurements* 32(1): 57–73, DOI 10.1016/S1350-4487(99)00253-X.

Roberts HM and Wintle AG, 2001. Equivalent dose determinations for polymineralic fine-grains using the SAR protocol: Application to a Holocene sequence of the Chinese Loess Plateau. *Quaternary Science Reviews* 20(5–9): 859–863, DOI 10.1016/S0277-3791(00)00051-2.

Thomsen KJ, Murray AS, Jain M and Bøtter-Jensen L, 2008. Laboratory fading rates of various luminescence signals from feldspar-rich sediment extracts. *Radiation Measurements* 43(9–10): 1474–1486, DOI 10.1016/j.radmeas.2008.06.002.